PCCP

Accepted Manuscript

ROYAL SOCIETY OF CHEMISTRY

www.rsc.org/pccp

Quantum Mechanical Study of the β- and δ-Lyase Reactions during the Base Excision Repair Process: Application to FPG

Shahin Sowlati-Hashjin[a] and Stacey D. Wetmore[a]*

Abstract

Bacterial FPG (or MutM) is a bifunctional DNA glycosylase that is primarily responsible for excising 8-oxoguanine (OG) from the genome by cleaving the glycosidic bond and the DNA backbone at the 3′- and 5′-phosphates of the damaged nucleoside. In the present work, quantum mechanical methods (SMD-M06-2X/6-311+G(2df,2p)//IEF-PCM-B3LYP/6-31G(d)) and a ring-opened Schiff base model that includes both the 3′- and 5′-phosphate groups are used to investigate the β- and δ-elimination reactions facilitated by FPG. Both the β- and δ-elimination reactions are shown to proceed through an E1cB mechanism that involves proton abstraction prior to the phosphate–ribose bond cleavage. Since transition states for the phosphate elimination reactions could not be characterized in the absence of leaving group protonation, our work confirms that the phosphate elimination reactions require protonation by a residue in the FPG active site, and can likely be further activated by additional active-site interactions. Furthermore, our model suggests that 5′-PO_4 activation may proceed through a nearly isoenergetic direct (intramolecular) proton transfer involving the O4′ proton of the deoxyribose of the damaged nucleoside. Regardless, our model predicts that both 3′- and 5′-phosphate protonation and elimination steps occur in a concerted reaction. Most importantly, our calculated barriers for the phosphate cleavage reactions reveal inherent differences between the β- and δ-elimination steps. Indeed, our calculations provide a plausible explanation for why the δ-elimination rather than the β-elimination is the rate-determining step in the BER facilitated by FPG, and why some bifunctional glycosylases (including the human counterpart, hOgg1) lack δ-lyase activity. Together, the new mechanistic features revealed by our work can be used in future large-scale modeling of the DNA–protein system to unveil the roles of key active sites residues in these relatively unexplored BER steps.

Introduction

Oxidation of guanine to form 8-oxoguanine (OG) is among the most common DNA damaging events,[1] occurring ~1000 times per cell per day.[2-4] Since the Hoogsteen face of OG can form a stable mispair with adenine, a canonical Watson-Crick G:C base pair can be converted into a T:A pair after two rounds of replication following OG formation. Thus, it is crucial to identify and replace OG with the native nucleobase. In cells, OG is primarily removed by the base excision repair (BER) process, which more generally excises many different damaged DNA nucleobases that deviate from the canonical analogues by only a few atoms.[5]

The chemical step of BER begins when a DNA glycosylase uses either an amine group of an active site residue (bifunctional glycosylase) or a water molecule (monofunctional glycosylase) to displace the damaged nucleobase, which produces an abasic site.[6, 7] During the deglycosylation step catalyzed by a bifunctional glycosylase, a Schiff base forms between the nitrogen of the nucleophile and C1′ of the sugar moiety, and the sugar ring opens. In the next (β-elimination) step, a proton bound to C_β is abstracted by a base and the 3′-phosphate with respect to the damaged nucleoside is eliminated (see, for example, Scheme 1(a) – (b)).[8] In addition to β-lyase activity, some bifunctional glycosylases possess δ-lyase activity, which expels the 5′-phosphate with respect to the damaged nucleoside after C4′–H abstraction (see, for example, Scheme 1(c) – (d)).[8] When the bifunctional glycosylase does not exhibit δ-lyase activity, 5′-phosphate elimination is facilitated by an AP-endonuclease. Regardless, the bifunctional glycosylase is recovered via hydrolysis of the DNA–protein crosslink. At the end of the repair process, a native nucleotide is added at the original damage site by a DNA polymerase and the DNA strand is sealed by a ligase.

To date, eight different DNA glycosylases have been identified in *E. coli* and ten in humans, each of which targets specific types of damaged nucleobases, with the substrate specificity overlapping in some cases.[9] Bifunctional formamidopyrimidine-DNA glycosylase (FPG or MutM) is primarily responsible for excising OG in bacteria. Although its human counterpart, hOgg1, is specific to OG and 2,6-diamino-4-hydroxy-5-formamidopyrimidine (FapyG), FPG also excises several other damaged nucleobases, such as thymine glycol (Tg), dihydrouracil (DHU) and 5-hydroxyuracil (5-OHU), as well as hydantoins.[9-13] FPG and hOgg1 also differ in the active site nucleophile that catalyzes the base excision step, which has been identified to be a proline residue (Pro2) for FPG compared to a lysine side chain (Lys249) for hOgg1. Interestingly, FPG is approximately 80-fold more efficient than hOgg1 at excising OG.[14] Moreover, although hOgg1 exhibits only weak β-lyase activity,[5, 15] FPG exhibits both β- and δ-lyase activity.[9]

The unique features of FPG compared to hOgg1 have attracted attention towards this bacterial enzyme. Despite an abundance of experimental studies on different aspects of the BER process facilitated by FPG,[13, 16-21] and structural information gained from available DNA–enzyme crystal structures,[22-24] several mechanistic features of the reactions catalyzed by FPG remain unclear and require further detailed investigation. Indeed, very little is known about the mechanism of action of the β- and δ-lyase reactions catalyzed by FPG. Specifically, the general base that abstracts the proton in the β-elimination reaction is currently unidentified.[9] A strong acceptor is required for this proton abstraction step despite the lower *p*Ka of C2′ in the Schiff base than the nucleotide.[9] A crystallographic water in the proximity of C2′ (3.5 Å) was suggested to play this role in *Geobacillus stearothermophilus* (*Bst*-FPG).[23] However, this molecule is not present in related enzymes, including *E. coli* FPG.[9] Although the excised OG has also been

proposed to facilitate proton abstraction in the case of hOgg1,[25, 26] it has been suggested that OG does not explain the overall efficiency of FPG.[9] Moreover, since OG is not present in a crystal structure of the borohydride-trapped DNA–protein crosslink, it has been proposed that excised OG is not tightly bound in the FPG active site, likely diffusing away after cleavage.[23] In addition to unknowns surrounding C4′ proton abstraction, there are currently no proposals for the identity of the general base that abstracts the C4′ proton in the δ-elimination reaction.

Although there has been some speculation about the general base that abstracts the protons, even fewer details are available about the phosphate elimination reaction. Crystal structures reveal that the 3′- and 5′-phosphates with respect to the damaged nucleoside are in close proximity to conserved residues in FPG.[23, 27] Specifically, the 3′-phosphate interacts with Lys57 and Arg259, while the 5′-phosphate interacts with Asn169, Arg259 and Tyr242.[23] Indeed, it has been proposed that Lys57 and Arg259 protonate the 3′- and 5′-phosphate moieties, respectively, while the other residues further stabilize the increased negative charge formed upon phosphate departure through hydrogen-bonding contacts.[23, 24] Although this evidence suggests that acidic residues in the proximity of the phosphate leaving groups are important for elimination, the reaction mechanisms for the excision steps have yet to be uncovered.

In light of the above experimental unknowns, several computational studies have investigated different aspects of the BER pathway facilitated by FPG.[28-35] Previous computational work includes molecular dynamics simulations of the *anti* (χ defined as ∠(O4′−C1′−N9−C4) equals 180 ± 90°) and *syn* (χ = 0 ± 90°) conformers of OG, (unmodified) G and several other lesions (such as FapyG, 4,6-diamino-5-formamidopyrimidine (FapyA), and 7,8-dihydro-8-oxoadenine (8-oxoA)) bound in the FPG active site, which shed light on the lesion binding modes and substrate interactions in the recognition pocket.[31-34] In addition, quantum

mechanical studies have investigated the catalytic reaction mechanism of the first BER step under the assumption that deglycosylation occurs prior to sugar ring opening.[29, 30] A recent combined experimental and computational study has characterized a deglycosylation mechanism involving ring opening preceding glycosidic bond cleavage.[36, 37] Beyond the initial deglycosylation step, several unique pathways for the β-elimination reaction were characterized in our lab using modified nucleoside-3′-monophosphate models and OG^- as the general base.[28, 38] However, the nucleoside-3′-monophosphate models employed in the previous studies were neutralized by a sodium ion,[28, 38] which prevents the phosphate protonation that has been proposed to facilitate the reaction.[23, 24] Furthermore, no computational study to date has considered the mechanism of action of the δ-elimination reaction.

The present work uses quantum mechanical methods and a small, yet chemically-relevant, model as a first step towards gaining currently missing information about the mechanistic details of the β- and δ-elimination reactions catalyzed by a bifunctional glycosylase during BER. In contrast to previous computational studies on the β-elimination step,[28, 38] anionic phosphate models are used to investigate the role of phosphate activation in the elimination reactions. Furthermore, our model simultaneously includes both 3′- and 5′-phosphate residues to allow the first comparison between the β- and δ-elimination reactions in attempts to reveal key mechanistic and energetic similarities and/or differences between these BER steps. This approach will unveil whether differences in the inherent chemistry helps explain why some bifunctional glycosylases only facilitate the β-elimination reaction. By using a simplistic model to characterize different potential pathways for the β- and δ-lyase reactions, the most relevant routes will be identified that can subsequently be considered using large-scale DNA–protein models in the future. Although we focus our discussion on FPG, our model choice allows our

results to be related to other bifunctional DNA glycosylases that use a proline residue to cleave the glycosidic bond, and that nick the DNA strand at the 3′- and 5′-sides of the damaged nucleoside (such as endonuclease VIII (Nei), Nei mammalian homologs (Nei-like: Neil)). Moreover, since the nature of the amine nucleophile has been shown to have negligible effects on the mechanism and energetics of the β-elimination step in the BER pathway,[28, 38] our current results for the 3′-phosphate elimination are valid for enzymes that employ a lysine nucleophile and exhibit only β-lyase activity (such as hOgg1, *E. coli* endonuclease III (Nth) and (human) hNTH1).

Computational Details

To simultaneously investigate the β- and δ-elimination reactions catalyzed by FPG, 1-[4-hydroxy-3,5-diyl dimethyl bis(phosphate)pentylidene] pyrrolidinium was used as the core component of our model (Scheme 2(a)). This component was built from the ring-opened deoxyribose intermediate optimized in our previous study[28] by replacing the 5′-methoxy group with a 5′-phosphate group. The 3′- and 5′-phosphates are capped with methyl groups in our model to avoid hydrogen bonding between the DNA backbone and nucleobase (OG) that cannot occur in the DNA–protein system. Support for our chosen starting model comes from a comparison between the associated relaxed structure and crystal structures of FPG bound to a borohydride-trapped abasic site (PDB ID: 1K82)[24] or a Schiff base intermediate (PDB ID: 1L1Z;[23] see Fig. S1, ESI). Specifically, deviations between our model and the crystal structures mainly arise due to crystallization techniques used to trap the DNA–protein crosslink (such as mutating key residue(s) or employing inhibitors), different C1′ hybridizations (sp^3 in the crystal

structures versus sp^2 in the optimized model), and the flexibility of the terminal phosphates in our model that are bound within a DNA oligomer in the crystal structures.

Similar to previous studies on the 3′-phosphate elimination BER step performed in our group,[28, 38] OG^- (or H–OG) is added to our model to act as the general base (or acid) as required for the reaction to proceed (Scheme 2(b)). Furthermore, OG^- can accept (or H–OG can deliver) a proton using either O8 or N9, and the associated pathways are denoted as O-base and N-base throughout the present work, respectively. Nevertheless, OG^- or H–OG is removed from the model for the reactions in which a general acid or base is not required. Similarly, the cleaved 3′-phosphate is removed from our model following the β-elimination step to prevent artificial interactions between the eliminated group and the remaining sugar–proline crosslink that are unlikely to occur in the DNA–protein system.

The reaction potential energy surfaces (PESs) were searched by characterizing transition states (TSs), and following the corresponding intrinsic reaction coordinate (IRC) in both (forward and backward) directions. All resulting stationary points were fully optimized at the B3LYP/6-31G(d) level of theory in the presence of bulk solvent as described by the IEF-PCM method implemented in Gaussian 09.[39] Since molecular simulations predict the dielectric constant to be $\varepsilon \approx 3$ in the center of globular proteins and increases gradually to up to $\varepsilon \approx 10$ at the boundary,[40-44] the dielectric was approximated as diethyl ether ($\varepsilon = 4.24$) in all calculations based on the shape of FPG and the active site location. Within our model, the product of some chemical steps (denoted as "primed" intermediates) do not exactly correspond to the reactant for the subsequent reaction due to inevitable translational motion of OG (the general base/acid) during the reaction. In these cases, the structure obtained from the reverse IRC was considered to be the intermediate for the previous reaction step. Unless otherwise mentioned, all reported

energies correspond to relative Gibbs energies obtained from single-point calculations at the SMD-M06-2X/6-311+G(2df,2p) level of theory, which include scaled (0.9806) zero-point vibrational energy and unscaled thermal corrections calculated at the optimization level of theory. All calculations were carried out using Gaussian 09 (Revision C.01).[39]

Results and Discussion

As outlined in the Introduction, the chemical steps facilitated by FPG include deglycosylation, ring opening, β-elimination and δ-elimination. In this study, we have focused on characterizing possible pathways for the β- and δ-elimination phases of BER facilitated by FPG (Scheme 3). The relative SMD-M06-2X/6-311+G(2df,2p) Gibbs energies for all reaction steps are provided in Tables 1 and 2, and the corresponding Gibbs reaction surfaces are shown in Fig. 1. The IEF-PCM-B3LYP/6-31G(d) relative energies (with and without (scaled) zero-point vibrational energy corrections) are provided in the ESI (Tables S1 – S4). In the sections below, important structural features of the stationary points and the energy barriers for all reaction pathways characterized are compared to each other and the literature when possible, and the biochemical implications of our findings that are important for future large-scale modeling on complete DNA–enzyme models are discussed.

β-Lyase Step

As described in the Introduction, the β-elimination reaction catalyzed by FPG occurs in conjunction with proton abstraction from C_β (C2′ of the deoxyribose) by a general base (Scheme

1(a)). Although either the *pro*-S-2′ or *pro*-R-2′ hydrogen can be abstracted in this step, structural information suggest that the elimination reaction proceeds by *pro*-S-2′ removal in *E. coli* FPG.[9] Specifically, the average (ν2) torsion angle around C1′–C2′–C3′–C4′ in *E. coli* FPG (ν2 = –81.6°) is close to the value required for *pro*-S-2′ removal through an *anti* stereochemical elimination (ν2 ≈ –60°).[9] Moreover, a previous computational study on the β-elimination reaction determined that *pro*-S-2′ abstraction has a smaller associated barrier than *pro*-R-2′.[38] Therefore, only *pro*-S-2′ removal was considered for the reaction facilitated by FPG in the present work.

In agreement with previous computational studies on the β-lyase step of BER,[28, 38] we find that the elimination reaction occurs in two successive steps with proton abstraction preceding phosphate cleavage (i.e., an E1cB mechanism). In our model, four different routes were characterized for the first *pro*-S-2′ abstraction step (Scheme 3). Specifically, the proton abstraction from the reactant (RC1) was considered to be facilitated by O8 (denoted as O-base) or N9 (denoted as N-base) of OG^-. Furthermore, since proton abstraction immediately follows deglycosylation, OG^- was placed in an orientation with respect to the rest of the model that corresponds to an *anti* or *syn* nucleoside conformation.

For O-base *pro*-S-2′ abstraction, the initial *syn* OG^- pathway led to a transition state with a similar structure (Fig. S2, ESI), but (~ 40 kJ/mol) higher barrier (Table S1, ESI), than isolated from an initial *anti* OG^- configuration. Thus, this pathway is not further discussed. Along the *anti* O-base *pro*-S-2′ abstraction pathway (Fig. 2, left), the transition state (TS1, Fig. 2, left) occurs with d(O8···H) = 1.246 Å, d(C2′···H) = 1.388 Å, and ∠(C2′···H···O8) = 174.3°. Both d(O8···H) and d(C2′···H) are slightly shorter (by 0.045 and 0.008 Å, respectively) than previously estimated using a nucleoside-3′-monophosphate model[28] since interactions between

the 5′-phosphate and OG^- (mainly N7–H) in our current model delay the TS. In the associated intermediate (IC1′; Fig. 2, left), the proton is completely transferred to OG (d(H–O8) = 0.992 Å) and a planar C3′–C2′–C1′–Nα arrangement is formed. H–OG maintains an N7–H···O interaction with the 5′-phosphate, which pulls H–OG away from C2′ (i.e., d(O8–H···C2′) = 2.114 Å compared to 2.063 Å in the absence of the 5′-phosphate).[28]

When C2′–H abstraction is facilitated by N9 (N-base pathway, Scheme 3), the proton abstraction barrier is significantly (~ 32 kJ/mol) lower when initiated with an *anti* rather than a *syn* OG^- orientation (Table S2, ESI). This difference mainly arises because the optimized reactant from the reverse IRC for the *syn* TS contains an intact glycosidic bond and an opened ring (Fig. S3, ESI). Thus, a larger calculated barrier arises for the *syn* than *anti* OG^- pathway since the barrier also accounts for the deglycosylation reaction. Although the deglycosylation BER step is not the focus of the current investigation, we acknowledge that there is a controversy in the literature surrounding the order of the deglycosylation and ring opening steps.[9, 36, 37] Using a similar model, our previous work suggests that (*syn* dOG) deglycosylation requires ~ 140 kJ/mol when occurring prior to ring opening.[28, 38] However, the current work predicts the calculated deglycosylation barrier to be 83.4 kJ/mol when occurring after ring opening in conjunction with C2′–H abstraction. Thus, our data suggests that the deglycosylation reaction can occur with a much lower energy barrier once the deoxyribose ring is opened. This finding is supported by the most recent experimental and computational studies on the deglycosylation of OG[36] and FapyG[37] facilitated by FPG, which proposed that an initial acid-catalyzed ring-opening step is followed by barrierless deglycosylation. Regardless, since the present investigation is concerned with the (β- and δ-) lyase activity of FPG, we focus our attention on the *anti* OG^- N-base pathway for β-lyase activity below.

In the *pro*-S-2′ abstraction transition state associated with the *anti* OG^- N-base pathway (TS1; Fig. 2, right), d(N9···H) = 1.400 Å and d(C2′···H) = 1.334 Å, which are comparable to the distances found using a model that lacks the C5′-phosphate moiety (d(N9···H) = 1.421 Å and d(C2′···H) = 1.320 Å). Furthermore, the ∠(C2′···H···N9) angle is 169.2°, which is only slightly (~ 2°) larger than previously obtained using the smaller model.[28] TS1 leads to an intermediate (IC1′; Fig. 2, right) with a planar C3′–C2′–C1′–Nα arrangement and H–OG in the proximity of the crosslink (d(N9–H··· C2′) = 2.288 Å). However, H–OG is further removed from the crosslink than in the intermediate associated with the O-base pathway (by 0.174 Å), likely due to repulsive contacts between O8 and the 5′-phosphate.

Comparison of the (*anti* OG^-) transition states for C2′–H abstraction facilitated by O8 and N9 reveals that d(N9···H) is significantly (0.154 Å) longer than d(O8···H), while the C2′···H distance is 0.058 Å shorter for the N-base than O-base pathway (Fig. 2). Moreover, the proton transfer occurs with a smaller angle for the N-base (∠(C2′···H···N9) = 169.4°) than O-base (∠(C2′···H···O8) = 174.3°) pathway. These structural differences result in a larger barrier for the N-base (51.5 kJ/mol) than O-base (22.0 kJ/mol) reaction. Although the O-base abstraction barrier is in good agreement with that calculated using a nucleoside-3′-monophosphate model and the same level of theory (21.5 kJ/mol), our N-base abstraction barrier is larger than in the absence of the 5′-phosphate (26.0 kJ/mol),[28] which may be due to destabilizing interactions between O8 and O5′ in the transition structure associated with the current model. In fact, in the N-base pathway, OG retains the initial *anti* orientation in the current study (Fig. 2), but rearranges to a *syn* orientation in the nucleoside-3′-monophosphate model, which leads to a stabilizing interaction between O5′ and N2–H.[28]

Following the proton abstraction step, the C3′–PO_4 bond cleavage completes the β-elimination reaction (Scheme 1(b)). Since a negatively charged phosphate is a poor leaving group, efforts to locate a transition state for the elimination reaction without protonating the phosphate group were unsuccessful. Indeed, the 3′-phosphate with respect to the damaged nucleoside is exposed to conserved Lys57 and Arg259 active site amino acids in crystal structures of FPG bound to DNA (Fig. 4(a)).[23, 24] The proposed mechanism for the C3′–PO_4 bond cleavage involves protonation of a terminal oxygen in the phosphate moiety by Lys57, with additional stabilization provided by Arg259.[24] In our model, free H–OG (i.e., OG^- formed following deglycosylation and C2′ proton abstraction by O8 (O-base) or N9 (N-base)) acts as the general acid to deliver a proton to the phosphate group (Scheme 3). To model this reaction step, H–OG was moved from the O5′-side in the intermediate from the C2′ abstraction step (IC1′; Fig. 2, left) to the O3′-side of the original deoxyribose moiety to generate IC1 (Fig. 3), the reactant for the C3′-phosphate activation/departure. Although activation was considered from both O8 and N9, the transition state for 3′-phosphate protonation by N9 could not be located, likely due to steric or electrostatic clashes between O8 of H–OG and O4′ of the sugar-phosphate backbone.

The 3′-phosphate protonation and elimination reactions are concerted (TS2, Fig. 3). In the transition state, d(O3′···C3′) = 1.529 Å and H–OG (O8) delivers the proton to the phosphate at an ∠(O8···H···O3′) angle equal to 164.4°, with d(O8···H) = 1.361 Å and d(H···O3′) = 1.103 Å. The d(O3′···C3′) distance in the transition state is significantly shorter than when the phosphate group is neutralized by a sodium ion (2.529 and 2.576 Å for the O-base and N-base pathways, respectively).[28] The calculated relative Gibbs energy for the 3′-phosphate cleavage step is 19.9 kJ/mol (Table 1). The β-elimination reaction results in an intermediate in which 3′-PO_4 is protonated at O3′ and the O3′–C3′ bond is completely cleaved (IC2, Fig. 3).

We emphasize that the 3′-phosphate elimination could only be characterized with our model once the leaving group was protonated, and our newly calculated barrier (19.9 kJ/mol) is significantly less than that previously reported when the phosphate moiety is solely stabilized by a sodium cation (80.7 – 95.4 kJ/mol).[28] Therefore, we anticipate that protonation of the phosphate moiety is required prior to expulsion, which is in-line with the elimination mechanism conjectured from experimental crystal structures.[24] Furthermore, this mechanism is supported by longer distances (weaker interactions) between the 3′-phosphate with respect to the damaged nucleoside and active site residues in hOgg1 (Fig. 4(b)),[25] which shows only weak β-lyase activity.[15] Interestingly, the contact distances between FPG active site residues (Lys57 and Arg259) and the 3′-phosphate are shorter to the terminal oxygen atoms (~ 2.5 – 3.1 Å) than O3′ (~ 4.9 – 5.1 Å) in the lesion recognition complex (PDB ID: 1R2Y),[45] as well as Schiff base (PDB ID: 1K82)[24] and abasic site (PDB ID: 1L1Z[23] and 3TWM[46]) intermediates (see Fig. 4(a)); however, all efforts to protonate a terminal oxygen atom of the phosphate group in our model were unsuccessful, and instead only O3′ could be protonated. Although this discrepancy could be an artifact of our computational model, this finding may suggest that active site residues adopt new positions as the reaction proceeds that alter active site–phosphate interactions compared with the static pictures provided by crystal structures or other species are involved in the reaction. For example, water molecules can be found in the proximity of the 3′-phosphate,[45, 47] which may protonate O3′. Regardless of the acid that protonates the phosphate group, additional stabilizing phosphate–enzyme interactions (Fig. 4(a)) may further lower the barrier height determined with our model. Therefore, the relative importance, dynamics and interplay of the multiple hydrogen bonds between FPG, active site water and the 3′-phosphate found in

experimental crystal structures must be more carefully considered using a complete DNA–enzyme model.

δ-Lyase Step

Current knowledge about the mechanism of the δ-lyase activity facilitated by FPG is even less than that for the β-lyase step. In parallel to the β-lyase reaction, it has been proposed that a (currently unidentified) base abstracts a proton from C4′ and, subsequently, the 5′-phosphate is eliminated (Scheme 1(c)–(d)).[9] Unlike for the β-elimination step, there is only one proton abstraction possibility (Scheme 4(a)). In our model, C4′–H is initially abstracted by either O8 or N9 of OG^- (Scheme 3), which produces a conjugated π-system over C4′–C3′–C2′–C1′–Nα (Fig. 5). The associated transition structure is earlier for the N-base than O-base pathway (TS3, Fig. 5), with d(C4′···H) being 0.023 Å shorter and d(X···H) being 0.101 Å longer (X = N9 for N-base and O8 for O-base pathway). The earlier TS for the N-base pathway may be due to hydrogen bonding between O4′–H and O8 of OG, which is not feasible along the O-base pathway since O4′–H is instead oriented towards the 5′-phosphate (TS3, Fig. 5). For the O-base pathway, OG^- abstracts the C2′ and C4′ protons with a similar angle (∠(C2′···H···O8) = 174.3° and ∠(C4′···H···O8) = 171.9°) in the β- and δ-elimination steps. In contrast, the proton abstraction angles differ by ~11° for the N-base pathway (∠(C2′···H···N9) = 169.2° and ∠(C4′···H···N9) = 158.2°), although both angles are smaller than in the corresponding O-base pathway. In the intermediate complex (IC3, Fig.4), O8 hydrogen bonds with O4′–H and N9–H interacts with 5′-PO_4 along the N-base pathway, while such specific interactions are absent in the O-base intermediate.

The energy barriers associated with proton abstraction in the δ-elimination step are 34.7 or 48.0 kJ/mol for the O-base or N-base pathways, respectively (Table 2). The higher barrier for the N-base pathway stems at least in part from hydrogen bonding between O4′–H and O8 in the associated reactant (RC2, Fig. 5). Both transition structures (TS3, Fig. 5) show bending of the sugar–phosphate moiety relative to the corresponding reactant (RC2). This bending occurs since it is energetically more favorable for the molecule to form an extended conjugated π-system after proton abstraction by aligning the *p*-orbital of C4′ in a parallel fashion with respect to the *p*-orbitals of C3′, C2′, C1′, and Nα (Scheme S1, ESI), which results in a highly stable intermediate (IC3, Fig. 5 and Table 2). The intermediate associated with the N-base pathway is more stable with respect to the corresponding reactant (–102.8 kJ/mol) than the O-base intermediate (–53.8 kJ/mol) due discrete hydrogen bonds between H–OG and the sugar-phosphate moiety. Although the C4′ and C2′ hydrogen abstraction barriers are similar for the N-base pathways (within 3 kJ/mol), the C4′–H abstraction pathway requires an additional 12 kJ/mol than C2′–H abstraction, likely due to the aforementioned bending in the transition state.

Similar to the β-elimination step, 5′-phosphate departure follows proton abstraction from the neighbouring (C4′) carbon. Furthermore, a transition state for the 5′-phosphate elimination could not be located in the absence of leaving group protonation. However, in the case of δ-elimination, efforts to protonate the phosphate group by (either O8 or N9) H–OG (the intermediate (IC3) following the C4′ abstraction step) were also unsuccessful. Instead, two unique pathways were characterized for 5′-PO_4 protonation/departure that involve the O4′ proton (Schemes 3 and 4). In the first (direct) pathway, 5′-PO_4 is activated through direct proton transfer from O4′ to O5′ (Scheme 4(c)). In the second (assisted) pathway, the O4′ proton is initially transferred to OG^- and 5′-PO_4 is then activated for departure at O5′ by H–OG (Scheme 4(c′) –

(c″)). Although technically either O8 or N9 could abstract the O4′ proton, only the N-base pathway could be characterized. Furthermore, in order for O4′–H abstraction to take place, H–OG in the previous intermediate (IC3) is replaced by OG^- in the reactant for the assisted pathway (RC3′).

In the transition state for O4′ proton abstraction along the assisted pathway (TS4′, Fig. 6), d(O4′···H) and d(H···N9) are 1.370 and 1.158 Å, respectively, and ∠(O4′···H···N9) = 171.6°. Similar to the β-elimination reaction, the phosphate protonation and cleavage steps are simultaneous in both the assisted (TS4″) and direct (TS4) pathways (Fig. 6). In the assisted pathway, d(O5′···C5′) = 2.452 Å, which is significantly longer than in the transition state for the β-elimination (d(O3′···C3′) = 1.529 Å) and slightly longer than in the direct pathway (d(O5′···C5′) = 2.310 Å). Furthermore, proton delivery occurs at a narrower angle (∠(O4′···H···O5′) = 145.8°) in the direct pathway compared to the assisted 5′-PO_4 cleavage (∠(N9···H···O5′) = 171.9°) and the β-elimination step (∠(O8···H···O3′) = 164.4°). The energy barrier for the 5′-PO_4 elimination is 188.6 kJ/mol for the direct route and 166.5 kJ/mol for the assisted pathway, which involves an additional 21.9 kJ/mol barrier associated with O4′ proton abstraction. This suggests that there is not an energetic preference for one pathway over the other within our model. The immediate product of the δ-elimination reaction is an enolate moiety (IC4′/IC4″), which rearranges to the final ketone product through a proton transfer from the expelled phosphate to C5′ (Scheme 4(d) – (e)). In the transition state (TS5, Fig. 7), the phosphate group delivers the proton with ∠(O5′···H···C5′) = 171.6°, d(O5′···H) = 1.512 Å and (C5′···H) = 1.200 Å. The associated calculated barrier is large (121.7 kJ/mol, Table 2) due to perturbation of the conjugated π-system upon protonation of C5′ (Scheme 4(d) – (e)), which completes the δ-lyase reaction (P, Fig. 7).

As discussed above, a transition state for the 5′-phosphate elimination reaction could not be isolated without phosphate protonation. Analysis of experimental crystal structures suggests that the 5′-phosphate interacts with Asn169, Arg259 and Tyr237 in the FPG active site (Fig. 4(a)), with Arg259 being proposed to protonate a terminal oxygen for phosphate departure.[23, 24] However, as discussed for 3′-phosphate elimination, efforts to locate a transition state corresponding to protonation of a terminal oxygen atom were unsuccessful and instead protonation only occurred at O5′ in our model. It is interesting to note that FPG active site residues are generally closer to O5′ (< 4.6 Å) than O3′ (< 5.3 Å) in a range of crystal structures,[23, 24, 45, 46] which may suggest that protonation of the 5′-phosphate at O5′ is more feasible. Nevertheless, the distances between the active site residues and terminal oxygen atoms in the 5′-phosphate group are shorter (up to 3.6 Å) than to O5′ (up to 4.6 Å) as discussed for the 3′-phosphate.

According to our model, the calculated barrier for the 5′-PO_4 elimination (166.5 – 188.6 kJ/mol) is significantly larger than anticipated for an enzyme-catalyzed reaction. Although this is likely in part due to the small size of our model, which neglects additional interactions with the 5′-phosphate occurring in the FPG active site, our results highlight the intrinsic low reactivity of the C5′–O5′ bond. As discussed for the 3′-PO_4 elimination step, larger computational models are required to elucidate the reaction mechanism and role of active site amino acids and/or solvent in this important process. Regardless, our calculated barrier for the δ-elimination step is much larger than determined for the β-elimination step (19.9 kJ/mol). This predicted difference between the β- and δ-elimination reactions is in agreement with experimental evidence suggesting that δ-elimination is the rate-determining step for OG removal by FPG.[48]

Furthermore, this observation may explain why bifunctional glycosylases that lack intensive interactions with 5′-PO_4 (such as hOgg1; Fig. 4(b)) do not show δ-lyase activity.[15]

Conclusion

In the current study, the β- and δ-elimination reactions facilitated by bifunctional glycosylases in the context of the base excision repair process were examined, with specific emphasis on bacterial FPG. Our model predicts that both the β- and δ-elimination reactions proceed through a step-wise (E1cB) mechanism in which (C2′ or C4′) proton abstraction is followed by cleavage of the phosphate backbone. Attempts to characterize the transition state corresponding to phosphate elimination without protonation were unsuccessful, and our model predicts phosphate protonation and elimination to be simultaneous events. In the case of 5′-side cleavage, two nearly isoenergetic pathways for phosphate protonation/elimination were characterized, which involved either (intramolecular) proton transfer from O4′ or protonation assisted by a general acid (OG^- in our model abstracts the O4′ proton and delivers the proton to the 5′-phosphate group). Regardless, our calculations suggest that the additional charge developing on the phosphate moiety must be highly stabilized in the glycosylase active site in order for the reaction to occur. It is anticipated that the multiple active site interactions with the phosphate groups seen in experimental crystal structures of FPG bound to DNA will further lower the barriers calculated with our model. Interestingly, our model indicates that O3′ and O5′ are intrinsically more likely to accept a proton than the terminal oxygen atoms of the phosphate group, which contradicts conclusions drawn from interaction distances measured in experimental crystal structures. Most importantly, the calculated barrier for 5′-phosphate elimination is larger

than for 3′-phosphate elimination. This intrinsic difference between the β- and δ-dephosphorylation reactions at least in part rationalizes why the δ-elimination is the rate-determining step for some bifunctional glycosylases (such as bacterial FPG) and explains why some bifunctional glycosylases do not exhibit δ-lyase activity (such as human hOgg1). Future work can use the reaction pathways characterized in the present study and large-scale DNA–protein models to investigate the effects of interactions with active site residues on the elimination reactions in order to verify our reported mechanisms and elucidate the roles of individual DNA–protein contacts.

Acknowledgement

Financial support was provided by the Natural Sciences and Engineering Council of Canada (NSERC), the Canada Research Chair program, and the Canada Foundation for Innovation (CFI). Computer resources were provided by NUCLEIC (New Upscale Cluster for Lethbridge to Enable Innovative Chemistry) and WestGrid, part of the Compute/Calcul Canada HPC platform.

Notes

[a] Department of Chemistry and Biochemistry, University of Lethbridge, 4401 University Drive West, Lethbridge, Alberta, T1K 3M4, Canada. E-mail: stacey.wetmore@uleth.ca

Electronic Supplementary Information (ESI) available: [Quantum Mechanical Study of the β- and δ-Lyase Reactions during the Base Excision Repair Process: Application to FPG DNA Glycosylase]. See DOI:

References

1. H. Kamiya, *Nucleic Acids Res.*, 2003, **31**, 517–531.
2. J. Cadet, T. Douki and J.-L. Ravanat, *Free Radic. Biol. Med.*, 2010, **49**, 9–21.
3. S. Kanvah, J. Joseph, G. B. Schuster, R. N. Barnett, C. L. Cleveland and U. Landman, *Acc. Chem. Res.*, 2010, **43**, 280–287.
4. B. van Loon, E. Markkanen and U. Hübscher, *DNA Repair*, 2010, **9**, 604–616.
5. S. C. Brooks, S. Adhikary, E. H. Rubinson and B. F. Eichman, *Biochim. Biophys. Acta*, 2013, **1**, 247–271.
6. J. T. Stivers and Y. L. Jiang, *Chem. Rev. (Washington, DC, U. S.)*, 2003, **103**, 2729–2759.
7. P. J. Berti and J. A. B. McCann, *Chem. Rev. (Washington, DC, U. S.)*, 2006, **106**, 506–555.
8. M. Bhagwat and J. A. Gerlt, *Biochemistry*, 1996, **35**, 659–665.
9. D. O. Zharkov, G. Shoham and A. P. Grollman, *DNA Repair*, 2003, **2**, 839–862.
10. C. J. Wiederholt, M. O. Delaney, M. A. Pope, S. S. David and M. M. Greenberg, *Biochemistry*, 2003, **42**, 9755–9760.
11. D. Gasparutto, E. Muller, S. Boiteux and J. Cadet, *Biochim. Biophys. Acta, Gen. Subj.*, 2009, **1790**, 16–24.
12. Z. Hatahet, Y. W. Kow, A. A. Purmal, R. P. Cunningham and S. S. Wallace, *J. Biol. Chem.*, 1994, **269**, 18814–18820.
13. J. Tchou, H. Kasai, S. Shibutani, M. H. Chung, J. Laval, A. P. Grollman and S. Nishimura, *Proc. Natl. Acad. Sci. U. S. A.*, 1991, **88**, 4690–4694.
14. G. Frosina, *Mol. Aspects Med.*, 2007, **28**, 323–344.
15. D. O. Zharkov, T. A. Rosenquist, S. E. Gerchman and A. P. Grollman, *J. Biol. Chem.*, 2000, **275**, 28607–28617.
16. N. A. Kuznetsov, C. Bergonzo, A. J. Campbell, H. Li, G. V. Mechetin, C. de los Santos, A. P. Grollman, O. S. Fedorova, D. O. Zharkov and C. Simmerling, *Nucleic Acids Res.*, 2014, DOI: 10.1093/nar/gku1300.
17. V. B. J. Tchou, S. Shibutani, I. Antoshechkin, J. Miller, A.P. Grollman, F. Johnson, *J. Biol. Chem.*, 1994, **269**, 15318–15324.
18. F. Coste, M. Ober, Y. V. Le Bihan, M. A. Izquierdo, N. Hervouet, H. Mueller, T. Carell and B. Castaing, *Chem. Biol.*, 2008, **15**, 706–717.
19. M. L. Hamm, T. J. Gill, S. C. Nicolson and M. R. Summers, *J. Am. Chem. Soc.*, 2007, **129**, 7724–7725.
20. J. Tchou and A. P. Grollman, *J. Biol. Chem.*, 1995, **270**, 11671–11677.
21. D. O. Zharkov, R. A. Rieger, C. R. Iden and A. P. Grollman, *J. Biol. Chem.*, 1997, **272**, 5335–5341.
22. F. Coste, M. Ober, T. Carell, S. Boiteux, C. Zelwer and B. Castaing, *J. Biol. Chem.*, 2004, **279**, 44074–44083.
23. J. C. Fromme and G. L. Verdine, *Nat. Struct. Biol.*, 2002, **9**, 544–552.

24. R. Gilboa, D. O. Zharkov, G. Golan, A. S. Fernandes, S. E. Gerchman, E. Matz, J. H. Kycia, A. P. Grollman and G. Shoham, *J. Biol. Chem.*, 2002, **277**, 19811–19816.
25. S. D. Bruner, D. P. G. Norman and G. L. Verdine, *Nature (London, U. K.)*, 2000, **403**, 859–866.
26. J. C. Fromme, S. D. Bruner, W. Yang, M. Karplus and G. L. Verdine, *Nat. Struct. Biol.*, 2003, **10**, 204–211.
27. D. O. Zharkov, G. Golan, R. Gilboa, A. S. Fernandes, S. E. Gerchman, J. H. Kycia, R. A. Rieger, A. P. Grollman and G. Shoham, *EMBO J.*, 2002, **21**, 789–800.
28. S. Sowlati-Hashjin and S. D. Wetmore, *J. Phys. Chem. B*, 2014, **118**, 14566–14577.
29. E. J. Shim, J. L. Przybylski and S. D. Wetmore, *J. Phys. Chem. B*, 2010, **114**, 2319–2326.
30. H.-W. T. Jun-Hua Zheng, Guang-Ju Chen, *Int. J. Quant. Chem.*, 2011, **111**, 2454–2463.
31. P. Amara, L. Serre, B. Castaing and A. Thomas, *Protein Sci.*, 2004, **13**, 2009–2021.
32. E. I. Zaika, R. A. Perlow, E. Matz, S. Broyde, R. Gilboa, A. P. Grollman and D. O. Zharkov, *J. Biol. Chem.*, 2004, **279**, 4849–4861.
33. R. A. Perlow-Poehnelt, D. O. Zharkov, A. P. Grollman and S. Broyde, *Biochemistry*, 2004, **43**, 16092–16105.
34. K. Song, V. Hornak, C. D. Santos, A. P. Grollman and C. Simmerling, *Biochemistry*, 2006, **45**, 10886–10894.
35. P. Amara and L. Serre, *DNA Repair*, 2006, **5**, 947–958.
36. K. Sadeghian, D. Flaig, I. D. Blank, S. Schneider, R. Strasser, D. Stathis, M. Winnacker, T. Carell and C. Ochsenfeld, *Angew. Chem. Int. Ed.,* 2014, **53**, 10044–10048.
37. I. D. Blank, K. Sadeghian and C. Ochsenfeld, *Scientific Reports*, 2015, DOI: 10.1038/srep10369.
38. J. L. Kellie and S. D. Wetmore, *J. Phys. Chem. B*, 2012, **116**, 10786–10797.
39. M. J. Frisch, G. W. Trucks, H. B. Schlegel, G. E. Scuseria, M. A. Robb, J. R. Cheeseman, G. Scalmani, V. Barone, B. Mennucci, G. A. Petersson, H. Nakatsuji, M. Caricato, X. Li, H. P. Hratchian, A. F. Izmaylov, J. Bloino, G. Zheng, J. L. Sonnenberg, M. Hada, M. Ehara, K. Toyota, R. Fukuda, J. Hasegawa, M. Ishida, T. Nakajima, Y. Honda, O. Kitao, H. Nakai, T. Vreven, J. A. M. Jr., J. E. Peralta, F. Ogliaro, M. Bearpark, J. J. Heyd, E. Brothers, K. N. Kudin, V. N. Staroverov, R. Kobayashi, J. Normand, K. Raghavachari, A. Rendell, J. C. Burant, S. S. Iyengar, J. Tomasi, M. Cossi, N. Rega, J. M. Millam, M. Klene, J. E. Knox, J. B. Cross, V. Bakken, C. Adamo, J. Jaramillo, R. Gomperts, R. E. Stratmann, O. Yazyev, A. J. Austin, R. Cammi, C. Pomelli, J. W. Ochterski, R. L. Martin, K. Morokuma, V. G. Zakrzewski, G. A. Voth, P. Salvador, J. J. Dannenberg, S. Dapprich, A. D. Daniels, O. Farkas, J. B. Foresman, J. V. Ortiz, J. Cioslowski and D. J. Fox, Gaussian, Inc., Wallingford CT, Revision C.01 edn., 2009.
40. M. K. Gilson and B. H. Honig, *Biopolymers*, 1986, **25**, 2097–2119.
41. H. Nakamura, T. Sakamoto and A. Wada, *Protein Eng.*, 1988, **2**, 177–183.
42. M. Karplus and J. A. McCammon, *CRC Crit. Rev. Biochem.*, 1981, **9**, 293–349.
43. T. Simonson, D. Perahia and A. T. Brunger, *Biophys. J.*, 1991, **59**, 670–690.
44. T. Simonson and D. Perahia, *Proc. Natl. Acad. Sci. USA*, 1995, **92**, 1082–1086.
45. J. C. Fromme and G. L. Verdine, *J. Biol. Chem.*, 2003, **278**, 51543–51548.
46. S. Duclos, P. Aller, P. Jaruga, M. Dizdaroglu, S. S. Wallace and S. Doublié, *DNA Repair*, 2012, **11**, 714–725.
47. L. Serre, K. P. De Jesus, S. Boiteux, C. Zelwer and B. Castaing, *EMBO J.*, 2002, **21**, 2854–2865.
48. O. S. Fedorova, G. A. Nevinsky, V. V. Koval, A. A. Ishchenko, N. L. Vasilenko and K. T. Douglas, *Biochemistry*, 2002, **41**, 1520–1528.

Table 1. Relative Gibbs energies (ΔG, kJ/mol) for stationary points characterized along the *anti* O-base and N-base pathways for the β-elimination reaction.[a]

Reaction Step	Stationary Point	O-base	N-base
C2′–H Abstraction	RC1	0.0	0.0
	TS1	22.0	51.5
	IC1	–0.6	–2.6
3′-PO_4 Elimination	TS2	19.3	-
	IC2	–18.7	-

[a] Relative energies were obtained with SMD-M06-2X/6-311+G(2df,2p)//IEF-PCM-B3LYP/6-31G(d) and include (scaled) zero-point vibrational energy and (unscaled) thermal corrections. See Figures 2 – 3 for the corresponding structural information.

Table 2. Relative Gibbs energies (ΔG, kJ/mol) for stationary points characterized along the O-base and N-base pathways for the δ-elimination reaction, as well as the enol-keto rearrangement.[a]

Reaction Step	Stationary Point	O-base	N-base
C4′–H Abstraction	RC2	0.0	0.0
	TS3	34.7	48.0
	IC3	–53.8	–102.8
		Direct	**Assisted**
5′-PO_4 Elimination	RC3/RC3′	0.0	0.0
	TS4′	-	21.9
	TS4/IC4′	188.6	18.8
	TS4″	-	185.3
	IC4/IC4″	78.9	92.0
Enol-keto Rearrangement	TS5	200.6	-
	P	176.8	-

[a] Relative energies were obtained with SMD-M06-2X/6-311+G(2df,2p)//IEF-PCM-B3LYP/6-31G(d) and include (scaled) zero-point vibrational energy and (unscaled) thermal corrections. See Figures 3 – 6 for the corresponding structural information.

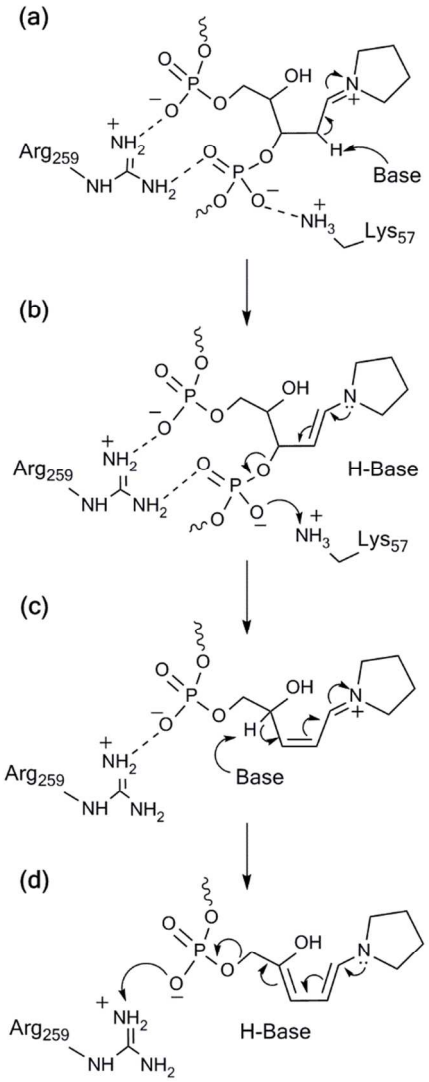

Scheme 1. Proposed chemical steps during β- and δ-lyase activity of FPG. Specifically, (a) an active-site base abstracts *pro*-S-2′, which is followed by (b) the elimination of the 3′-phosphate. Subsequently, (c) C4′–H is removed by a general base and (d) δ-elimination occurs. In FPG, the 3′-phosphate has been proposed to be protonated by Lys57 and further stabilized by Arg259, while the 5′-phosphate has been proposed to be protonated by Arg259 and further stabilized by Tyr237 and Asn169. Asn169 and Tyr237 are not shown for clarity.

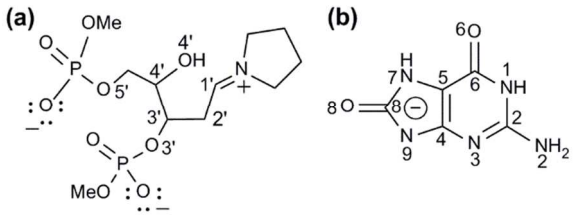

Scheme 2. 2D representation and atomic numbering of a) 1-[4-hydroxy-3,5-diyl dimethyl bis(phosphate)pentylidene] pyrrolidinium, and b) the negatively charged OG employed in our initial computational model.

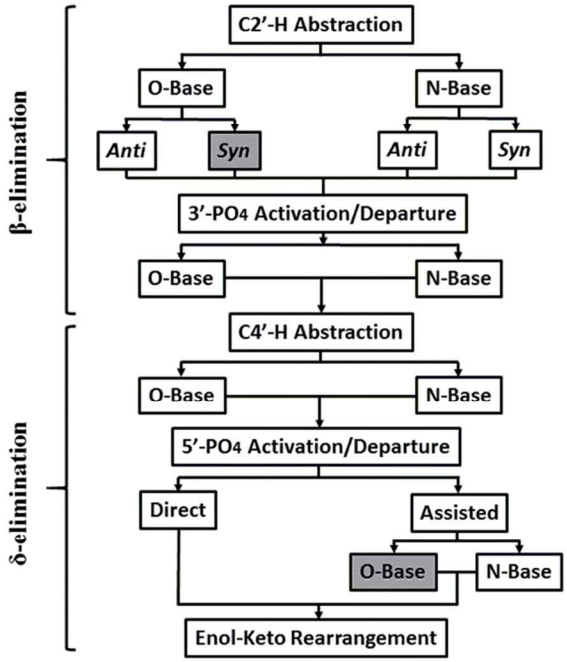

Scheme 3. Pathways for β- and δ-elimination facilitated by FPG considered in the present study.

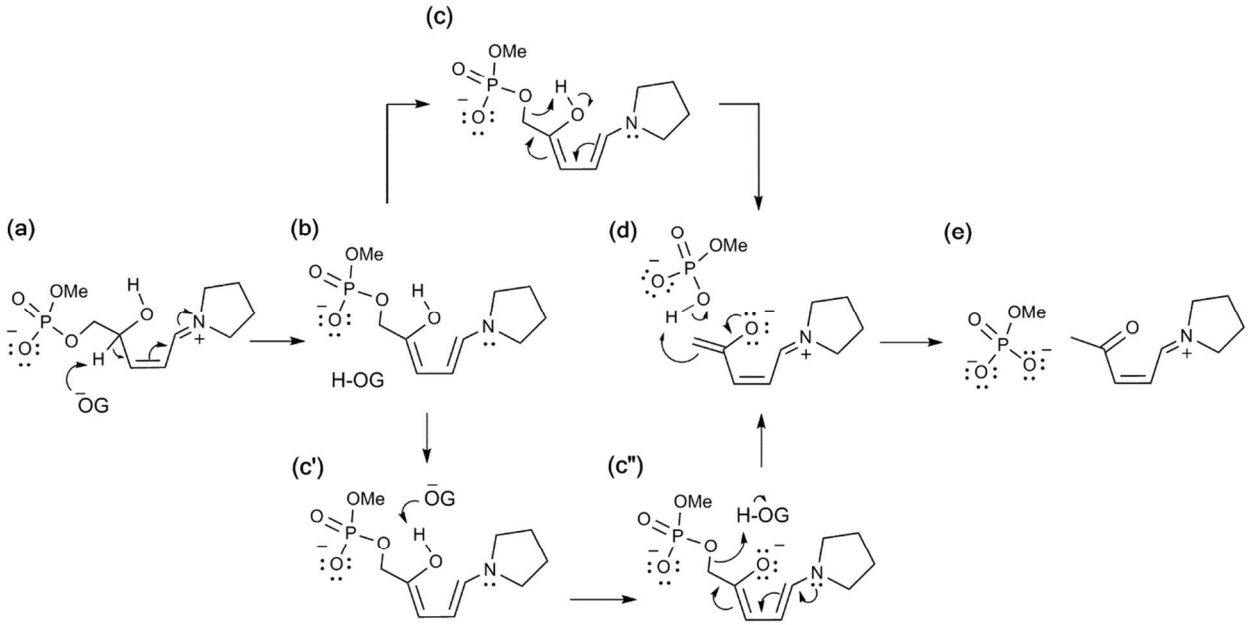

Scheme 4. Pathways characterized in this study for the δ-elimination reaction facilitated by FPG, including direct ((b) – (c)) and assisted ((b) – (c') – (c")) phosphate protonation/elimination routes.

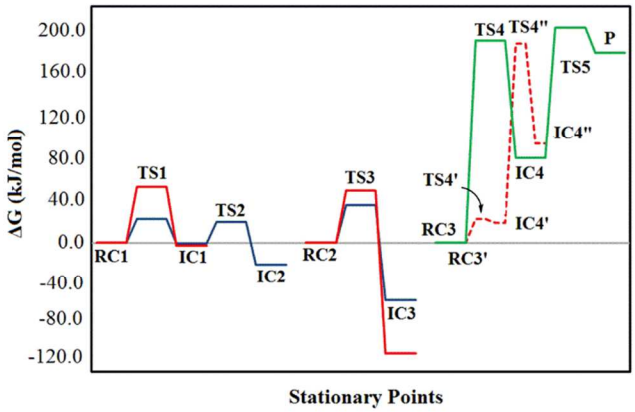

Fig. 1 The SMD-M06-2X/6-311+G(2df,2p)//IEF-PCM-B3LYP/6-31G(d) Gibbs energies (kJ/mol) relative to the corresponding reactant for each pathway considered in the present study, including the N-base (red, solid), O-base (blue, solid), the N-base assisted 5′-PO_4 elimination (red, dashed), and the direct 5′-PO_4 elimination followed by enol-keto rearrangement (green, solid).

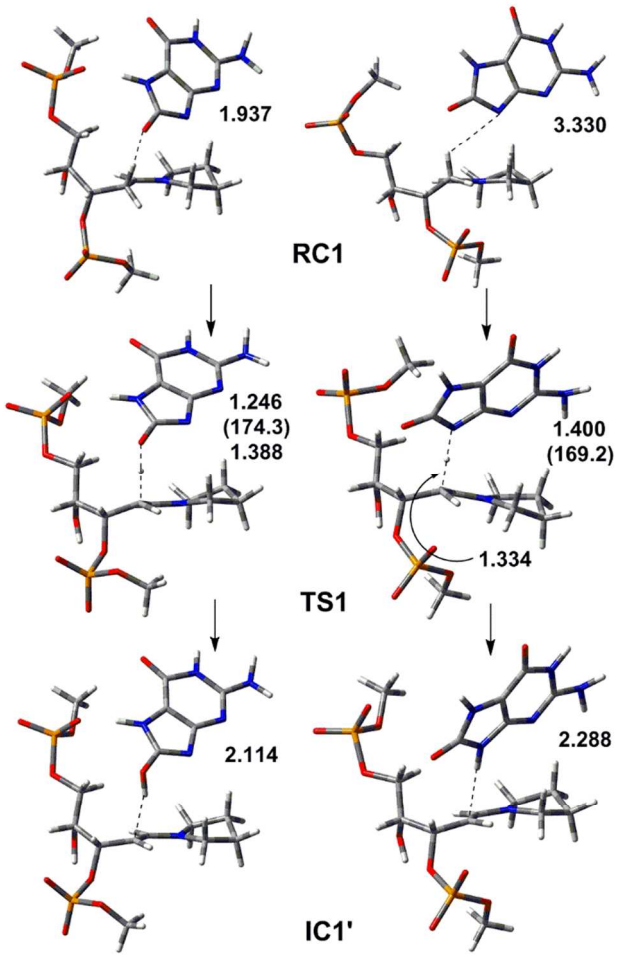

Fig. 2 Structures characterized along the *anti* O-base (left) and *anti* N-base (right) pathways for the C2′–H abstraction reaction. Important distances (Å) and angles (deg, in parentheses) obtained with IEF-PCM-B3LYP/6-31G(d) are provided.

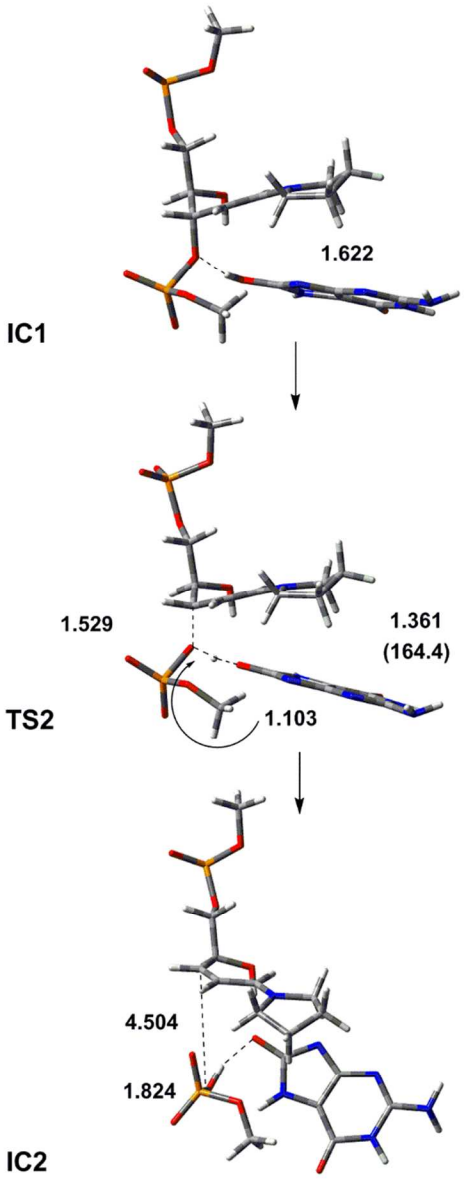

Fig. 3 Structures characterized along the O-base pathway for the 3′-PO_4 activation/elimination reaction. Important distances (Å) and angles (deg, in parentheses) obtained with IEF-PCM-B3LYP/6-31G(d) are provided.

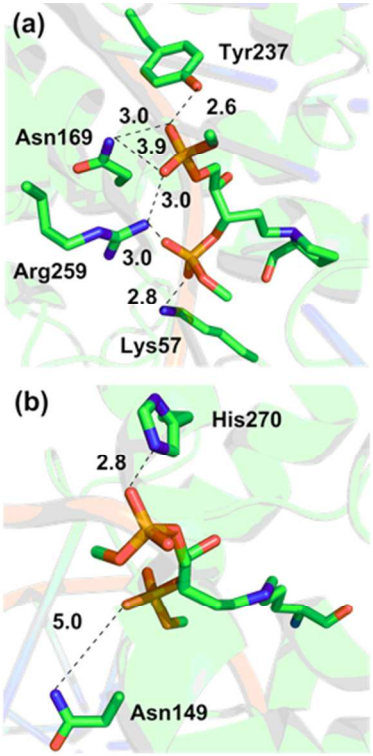

Fig. 4 Interactions between active site residues, and the 3′- and 5′-phosphate groups in a) FPG (PDB ID: 1L1Z) and b) hOgg1 (PDB ID: 1LWY). Select distances (Å) are provided. Main chain residues and water molecules are not shown for clarity.

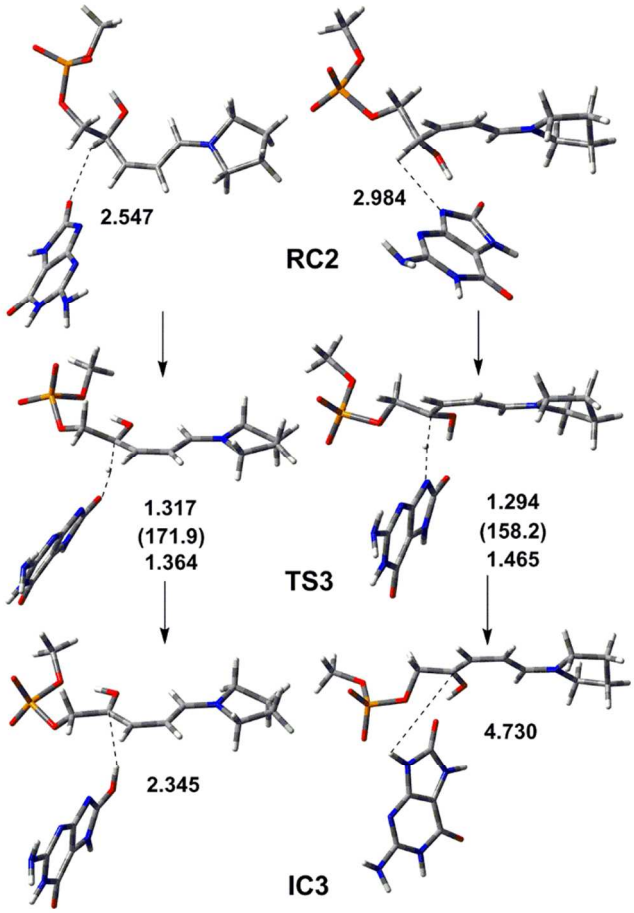

Fig. 5 Structures characterized along the O-base (left) and N-base (right) pathways for the C4′–H abstraction reaction. Important distances (Å) and angles (deg, in parentheses) obtained with IEF-PCM-B3LYP/6-31G(d) are provided.

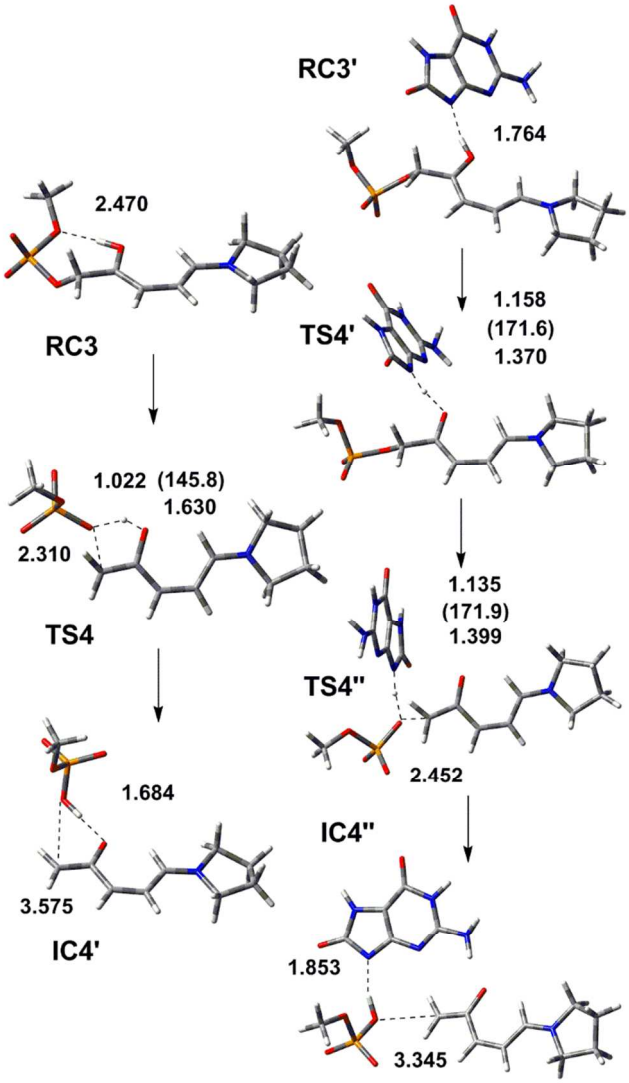

Fig. 6 Structures characterized along the direct (left) and acid-assisted (right) pathways for the 5′-PO_4 activation/elimination reaction. Important distances (Å) and angles (deg, in parentheses) obtained with IEF-PCM-B3LYP/6-31G(d) are provided.

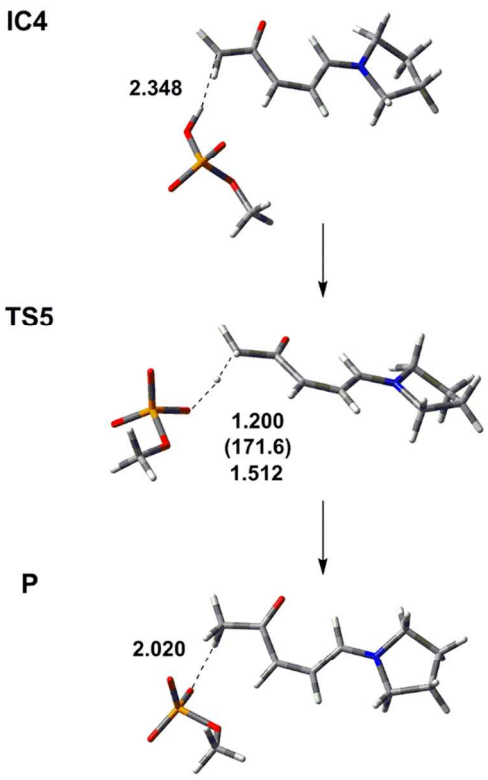

Fig. 7 Structures characterized for the enol-keto rearrangement step. Important distances (Å) and angles (deg, in parentheses) obtained with IEF-PCM-B3LYP/6-31G(d) are provided.

Graphic TOC

The β- and δ-elimination reactions catalyzed by FPG during the base excision repair of 8-oxoguanine are intrinsically different.